Structural and dielectric properties of Sr_2TiO_4 from first principles

Craig J. Fennie and Karin M. Rabe
Department of Physics and Astronomy, Rutgers University, Piscataway, New Jersey 08854-8019, USA
(Received 16 May 2003; published 21 November 2003)

We have investigated the structural and dielectric properties of Sr_2TiO_4, the first member of the $Sr_{n+1}Ti_nO_{3n+1}$ Ruddlesden-Popper series, within density-functional theory. Motivated by recent work in which thin films of Sr_2TiO_4 were grown by molecular beam epitaxy on $SrTiO_3$ substrates, the in-plane lattice parameter was fixed to the theoretically optimized lattice constant of cubic $SrTiO_3$ ($n=\infty$), while the out-of-plane lattice parameter and the internal structural parameters were relaxed. The fully relaxed structure was also investigated. Density-functional perturbation theory was used to calculate the zone-center phonon frequencies, Born effective charges, and the electronic dielectric permittivity tensor. A detailed study of the contribution of individual infrared-active modes to the static dielectric permittivity tensor was performed. The calculated Raman and infrared phonon frequencies were found to be in agreement with experiment where available. Comparisons of the calculated static dielectric permittivity with experiments on both ceramic powders and epitaxial thin films are discussed.

DOI: 10.1103/PhysRevB.68.184111 PACS number(s): 77.22.Ch, 63.20.Dj, 61.66.Fn

I. INTRODUCTION

Nonstoichiometric $SrTiO_3$ resists the formation of point defects by forming crystallographic shear (CS) phases.[1] For excess SrO, these CS phases form the $Sr_{n+1}Ti_nO_{3n+1}$ Ruddlesden-Popper (RP) series. The structures of the members of the RP series can be viewed as a stacking of SrO-terminated $SrTiO_3$ perovskite [001] slabs with relative shifts of $(a_0/2)$ [110], the slabs in the nth member of the series having a thickness of n cubic perovskite lattice constants. This representation of the structure for $n=1$ is shown in Fig. 1(a).

Considerable fundamental and practical interest in the RP series arises from the dielectric properties of its end member $SrTiO_3$ ($n=\infty$). Strontium titanate is an incipient ferroelectric with a high dielectric constant that can be readily tuned by applying a small dc bias. $SrTiO_3$ has low dielectric loss at microwave frequencies but a large temperature coefficient of dielectric constant (TCF). The prospect of ''engineering'' the properties of the constituent $SrTiO_3$ layers by varying n has stimulated the synthesis and study of the dielectric properties of various members of the RP series. Through the use of conventional ceramic processing techniques, single phase Sr_2TiO_4 ($n=1$),[1–5] $Sr_3Ti_2O_7$ ($n=2$),[1,3–6] and $Sr_4Ti_3O_{10}$ ($n=3$),[3] were formed. Recently, thin films of the first five members of the RP series were grown by molecular-beam epitaxy (MBE) on $SrTiO_3$ substrates.[7,8] Sr_2TiO_4, $Sr_3Ti_2O_7$, and $Sr_4Ti_3O_{10}$ were found to be nearly single phase while $Sr_5Ti_4O_{13}$ and $Sr_6Ti_5O_{16}$ films showed noticeable antiphase boundaries and intergrowth defects.[8] The dielectric properties of the $n=1$, 2, and ∞ ceramic samples have been characterized by various groups.[4,5,9,10] The dielectric properties of the $n=3$ and 4 ceramic samples have also been studied but these were believed not to be single phase.[5] It was found that $SrTiO_3$ had both the highest dielectric constant, ϵ_r, and the largest TCF of the RP series. Conversely, Sr_2TiO_4 was found to have the lowest ϵ_r of the series but also the lowest TCF (an order of magnitude smaller than $SrTiO_3$) while having a dielectric loss comparable to $SrTiO_3$. For thin films, Haeni *et al.*[8] performed low-frequency and microwave experiments to measure the dielectric permittivity of Sr_2TiO_4 and of $Sr_3Ti_2O_7$, to be discussed below.

Here we take the first step in understanding the dielectric behavior of the $Sr_{n+1}Ti_nO_{3n+1}$ Ruddlesden-Popper (RP) series from first principles by presenting our study of the structural and dielectric properties of Sr_2TiO_4 ($n=1$) using density-functional theory (DFT) structural optimization as well as density-functional perturbation theory (DFPT). DFT and DFPT have proved to be useful tools in investigating the structure, dynamical, and dielectric properties of metals and insulators, including complex oxides (see Ref. 11 for a review). In Sec. II we give the details of our DFT/DFPT calculations and describe various constraints that we imposed on the Sr_2TiO_4 structure. In Sec. III the results of our calculations for the ground-state structural parameters, Born effective charges, zone-center phonons, and electronic and static dielectric permittivity tensors at $T=0$ are presented and compared with experiment. In Sec. IV we discuss the sensitivity of the dielectric response to structural constraints and, through comparison with $SrTiO_3$, arrive at an understanding

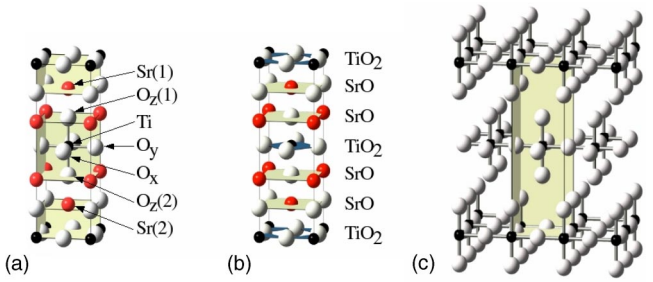

FIG. 1. (Color online) The structure of Sr_2TiO_4 (space group $I4/mmm$) can be viewed as (a) a stacking of SrO-terminated $SrTiO_3$ perovskite [001] slabs, (b) a stacking of TiO_2 and of SrO planes along [001], and (c) a series of Ti-O chains, infinitely long in the plane along [100] and [010], and of finite extent along [001] (the Sr atoms have been removed for clarity).

TABLE I. Wyckoff positions for Sr_2TiO_4.

Atom	Wyckoff position and point symmetry	Coordinates
Ti	$(2a)$ $4/mmm$	0,0,0
O_x, O_y	$(4c)$ mmm	$\frac{1}{2}$,0,0; 0,$\frac{1}{2}$,0
O_z	$(4e)$ $4mm$	$0,0,\pm z_{Oz}$
Sr	$(4e)$ $4mm$	$0,0,\pm z_{Sr}$

of the dielectric response and its anisotropy in the RP phases. Finally, in Sec. V we summarize our results and main conclusions.

II. METHOD

A. First-principles calculations

First-principles density-functional calculations were performed within the local-density approximation (LDA) as implemented in the ABINIT package.[12,13] The exchange-correlation energy is evaluated using the Teter rational polynomial fit to the Ceperley-Alder electron-gas data.[14] Teter extended norm-conserving pseudopotentials were used with Ti($3s$,$3p$,$4s$,$3d$), Sr($4s$,$4p$,$5s$), and O($2s$,$2p$) levels treated as valence states. The electronic wave functions were expanded in plane waves up to a kinetic energy cutoff of 35 Ha. Integrals over the Brillouin zone were approximated by sums on a $6\times6\times2$ mesh of special k points.[15]

B. Structural constraints

We first performed full optimization of the lattice parameters and internal coordinates in the reported structure of Sr_2TiO_4,[2] the body-centered-tetragonal K_2NiF_4 structure [space group $I4/mmm(D_{4h}^{17})$], with the primitive unit cell containing one formula unit as shown in Fig. 1. Ti atoms occupy Wyckoff position $(2a)$, O_x and O_y atoms $(4c)$, and Sr and O_z atoms $(4e)$, the latter with one free parameter (displacement along $\hat{z}$) each (see Table I). This yields the predicted structure under zero stress, roughly corresponding to bulk ceramic powders and relaxed epitaxial films. The structural relaxation was performed using a modified Broyden-Fletcher-Goldfarb-Shanno (BFGS) algorithm[16] to optimize the volume and atomic positions, followed by an optimization of the c/a ratio. This procedure was repeated to ensure convergence. The residual Hellmann-Feynman forces were less than 2 meV/Å . A second structure was considered to investigate the effects of epitaxial strain induced by the $SrTiO_3$ substrate on a fully coherent thin film. With the same space group, we fixed the in-plane lattice parameter to that of $SrTiO_3$ calculated within the present theory ($a=3.846$ Å),[17] while optimizing the other structural parameters: the c lattice constant and displacements along [001]. This was followed by ionic relaxation until the residual Hellmann-Feynman forces were less than 1 meV/Å.

The next section will show that the fully optimized lattice parameters are underestimated relative to the experimental values, a common feature in LDA calculations.[18] To investigate whether our calculations of the dielectric response of Sr_2TiO_4 are sensitive to this underestimation of the volume, two additional structures were considered. First, with the same space group, we optimized all internal coordinates fixing both the a and c lattice constants to values obtained by uniformly expanding the lattice constant of the in-plane constrained structure using the measured thermal-expansion coefficient of $SrTiO_3$ (Refs. 19 and 20) ($\alpha\approx7\times10^{-6}$/K) and a temperature increase of 300 K. We also optimized internal coordinates fixing both the a and c lattice constants to the values experimentally obtained for the thin-film sample. In both structures the ions were relaxed until the residual Hellmann-Feynman forces were less than 1 meV/Å.

C. Linear-response calculations

Linear-response methods provide an efficient means for computing quantities that can be expressed as derivatives of the total energy E with respect to a perturbation, such as that produced by displacement $u_{i\alpha}$ of an atom or a homogeneous electric field $\mathcal{E}$. Examples computed in this work include the force-constant matrix elements

$$\left.\frac{\partial^2 E}{\partial u_{i\alpha}\partial u_{j\beta}}\right|_0,$$

where $u_{i\alpha}$ is the displacement of atom i in Cartesian direction α from its position in the equilibrium crystal structure, the Born effective charge tensor

$$Z^*_{i\alpha\beta}=-\frac{\partial^2 E}{\partial d_{i\alpha}\partial\mathcal{E}_\beta},$$

where $d_{i\alpha}$ is the uniform displacement of the atomic sublattice i in Cartesian direction α from its position in the equilibrium unit cell, with derivatives taken in zero macroscopic field, and the electronic susceptibility tensor

$$\chi_{\alpha\beta}=-\frac{1}{V}\frac{\partial^2 E}{\partial\mathcal{E}_\alpha\partial\mathcal{E}_\beta},$$

which is related to the electronic dielectric permittivity tensor ϵ_∞ by $\epsilon_\infty=1+4\pi\chi$, where V is the volume of the primitive unit cell. In this work, we compute these derivatives using the variational formulation of density-functional perturbation theory (DFPT), implemented in the ABINIT package.[13,21,22]

The static dielectric permittivity tensor ϵ_0 can be obtained directly from the quantities computed by DFPT. In general, the static dielectric permittivity tensor of a nonpolar material can be written[23,24] as the sum of the electronic dielectric permittivity tensor ϵ_∞ and a sum of contributions $\Delta\epsilon_m$ from each of the zone-center polar modes m:

$$\epsilon^0_{\alpha\beta}=\epsilon^\infty_{\alpha\beta}+\sum_m \Delta\epsilon_{m,\alpha\beta}, \tag{1}$$

where $\Delta\epsilon_m$ is given by[25,26]

$$\Delta\epsilon_{m,\alpha\beta}=\frac{4\pi e^2}{M_0 V}\frac{\tilde{Z}^*_{m\alpha}\tilde{Z}^*_{m\beta}}{\omega_m^2} \tag{2}$$

TABLE II. Structural parameters of Sr_2TiO_4. (a) Fully relaxed cell. (b) Relaxation along the *c* axis, with *a* lattice constant fixed at theoretical $SrTiO_3$. (c) Relaxation with lattice constants fixed at values corrected for thermal expansion. (d) Lattice constants fixed at experimental (Ref. 7). Lattice constants, bond lengths, and internal parameters are in Å.

	Experimental			Present theory				Previous theory		
	Ceramic[a]	Ceramic[b]	Thin film[c]	(a)	(b)	(c)	(d)	Ref. 51[d]	Ref. 34[e]	Ref. 52[f]
Lattice constants										
a	3.88	3.88	3.88	3.822	3.846	3.855	3.88	3.942	4.0	3.892
c	12.60		12.46	12.32	12.27	12.30	12.46	12.56	12.68	12.70
c/a	3.247		3.211	3.223	3.190	3.190	3.211	3.186	3.17	3.263
Bond lengths										
Ti-O_x		1.94		1.911	1.923	1.928	1.940		2.0	
Ti-O_z		1.92		1.967	1.960	1.962	1.974		2.0	
Sr-O_z		2.56		2.402	2.397	2.406	2.455		2.47	
Internal parameters										
δ_{SrO}				0.176	0.182	0.180	0.173		0.12	
u'				1.879	1.869	1.872	1.888		1.94	
v				2.402	2.397	2.406	2.455		2.47	
Reduced coordinates										
z_{Oz}				0.160	0.160	0.160	0.158		0.158	
z_{Sr}				0.355	0.355	0.355	0.355		0.353	

[a]References 1–4.
[b]Reference 35.
[c]Reference 7.
[d]*Ab initio*, DFT, GGA.
[e]Semiempirical Hartree-Fock.
[f]Empirical atomistic simulations.

Here, M_0 is a reference mass taken as 1 amu. $(4\pi e^2/M_0V)\tilde{Z}^*_{m\alpha}\tilde{Z}^*_{m\beta}$ can be thought of as an effective plasma frequency, $\Omega^2_{p,m}$, of the mth normal mode,[27,28] while ω_m is the frequency of vibration of normal mode m. $\tilde{Z}^*_{m\alpha}$, which has been referred to as a mode effective charge,[29–31] is given by

$$\tilde{Z}^*_{m\alpha} = \sum_{i\gamma} Z^*_{\alpha\gamma}(i)\left(\frac{M_0}{M_i}\right)^{1/2}\xi_m(i\gamma), \tag{3}$$

where ξ_m is the dynamical matrix eigenvector; the corresponding real space eigendisplacement of atom i along β is given by $U_m(i\beta) = \xi_m(i\beta)/M_i^{1/2}$.[32] Thus we see that large lattice contributions to the static dielectric permittivity tensor are expected if the relevant mode frequencies are very low and/or if the effective plasma frequencies are large (reflecting large mode effective charges).

This formalism has been applied in a first-principles context in numerous calculations of the zero-temperature static dielectric response (for a review, see Ref. 33) in simple and complex oxides. For example, recent calculations for zircon ($ZrSiO_4$) (Ref. 23) and zirconia (ZrO_2) (Refs. 24 and 29) yield good agreement with experiment.

III. RESULTS

A. Crystal structure of Sr_2TiO_4

The reported crystal structure of Sr_2TiO_4 can also be viewed as a stacking of TiO_2 and SrO planes along [001] as shown in Fig. 1(b), the stacking sequence being TiO_2-SrO-SrO where the second SrO layer is shifted with respect to the previous SrO layer by $\frac{1}{2}a_0$ along [110]. In previous work,[34] the internal structural parameters are presented as u' and v, the distance between TiO_2 and SrO planes and between successive SrO planes, respectively, and δ, the distance along c between Sr and O in the same SrO layer, which quantifies the ''rumpling'' of the layer.

In Table II we present the theoretical lattice parameters for the structures discussed in Sec. II and compare them with the experimental values for ceramic samples[2,4,35] and for thin films epitaxially grown on $SrTiO_3$ ($a = 3.905$ Å) substrates.[7,8] The lattice constants of the fully relaxed structure, Table II, column (a), are smaller than the measured lattice constants of the ceramic powder. Specifically, the a lattice parameter was calculated to be less than experiment by 1.5%, which is within the error typically associated with the LDA, while the c lattice parameter is underestimated by 2.2%. The smaller value of c measured for the thin-film samples reduces this discrepancy to 1.1%. There is considerable rumpling of the SrO layers, $\delta_{SrO} = 0.05a_0$. This rumpling is such that the O_z and Sr atoms move in a direction away from and towards the TiO_2 layers, resulting in a Ti-O_z bond slightly larger (2.9%) than the Ti-O_y (or equivalently Ti-O_x) bond. As pointed out by Noguera, Ruddlesden and Popper had assumed that this rumpling was equal to zero. The present study supports the previous calculation[34] by finding a nonzero rumpling. The experimental work of Venkateswaran *et al.*[35] also suggested a nonzero rumpling of the

TABLE III. Nonzero components of the calculated Born effective charge tensors Sr_2TiO_4.

	(a)			(b)			(c)			(d)		
Atom	Z^*_{xx}	Z^*_{yy}	Z^*_{zz}	Z^*_{xx}	Z^*_{yy}	Z^*_{zz}	Z^*_{xx}	Z^*_{yy}	Z^*_{zz}	Z^*_{xx}	Z^*_{yy}	Z^*_{zz}
Ti	6.96	6.96	5.14	6.89	6.89	5.20	6.88	6.88	5.20	6.88	6.88	5.15
O_y	−2.04	−5.46	−1.56	−2.05	−5.40	−1.55	−2.04	−5.40	−1.55	−2.04	−5.42	−1.52
Sr	2.37	2.37	2.75	2.36	2.36	2.76	2.36	2.36	2.75	2.37	2.37	2.72
O_z	−2.09	−2.09	−3.74	−2.08	−2.08	−3.79	−2.07	−2.07	−3.78	−2.08	−2.08	−3.75

SrO layer ($\delta_{SrO}=0.10$),[36] but found that the Ti-O_z bond is shorter than the Ti-O_y bond.

Next, we consider the structure in which we constrained the in-plane lattice constant to that of theoretical $SrTiO_3$ ($a=3.846$ Å), Table II column (b). This places the system under tensile in-plane stress equal to that of an experimental sample of Sr_2TiO_4 coherently matched to $SrTiO_3$ (lattice mismatch 0.6%). As can be seen in Table II, this has almost no effect on the optimized values of the other structural parameters, including c.

Finally, we consider the optimized structural parameters for the two expanded structures. The slight thermal expansion of the in-plane constrained structure has a correspondingly slight effect on the internal parameters, while the expanded c of the experimental thin-film structure has a larger effect. We see that a roughly homogeneous expansion of the lattice, i.e., column (a)→(d) and (b)→(c), decreases the rumpling of the SrO layer.

B. Born effective charge tensors

In the Sr_2TiO_4 structure, the site symmetries of the Ti atom, occupying Wyckoff position $2a$, and the O_z and Sr atoms, both occupying Wyckoff position $4e$, are tetragonal, while that of the O_x and O_y atoms, Wyckoff position $4c$, is orthorhombic. As a result, all Z^*'s are diagonal with two [Z^*(Ti), $Z^*(O_z)$, and Z^*(Sr)] and three [$Z^*(O_y)$ and $Z^*(O_x)$] independent components. Table III displays the diagonal components of the calculated Born effective charge tensors in Sr_2TiO_4 for the four structures considered. We see that the Z^*'s are relatively insensitive to the various volume and strain constraints imposed, consistent with what was shown for isotropic volume changes in $BaTiO_3$,[37] and for pure tetragonal strain in $KNbO_3$.[38] Also, we note an anomalously large value for $Z^*_{xx}(\mathrm{Ti})=Z^*_{yy}(\mathrm{Ti})$ (nominal charge $+4$) and for $Z^*_{xx}(O_x)=Z^*_{yy}(O_y)$ (nominal charge -2), these being the components of the Z^*'s corresponding to motion parallel to the Ti-O bond along a direction in which the infinite Ti-O chains have been preserved. In contrast, the anomalous parts of Z^*_{zz}(Ti) and $Z^*_{zz}(O_z)$, which again correspond to motion parallel to the Ti-O bond, but along [001] where the Ti-O bonds do not form continuous chains, are found to be less than half of those along the continuous Ti-O chain.

C. Phonon frequencies at Γ

For the Sr_2TiO_4 structure, group-theoretical analysis predicts that the 18 zone-center optic modes transform according to the following irreducible representations:

$$\Gamma_{optic}=2A_{1g}\oplus 2E_g\oplus 3A_{2u}\oplus 4E_u\oplus B_{2u}, \quad (4)$$

of which the A_{1g} and E_g modes are Raman active, the A_{2u} and E_u modes are infrared active, and the B_{2u} mode is neither Raman nor infrared active. By using projection operator methods, it can be shown that the A_{1g}, A_{2u}, and B_{2u} modes involve motion along [001] while in the E_g and E_u modes, atoms move along [100] and [010]. A complete listing of the symmetry adapted lattice functions is given in Refs. 39 and 40.

Table IV displays our calculated frequencies and mode assignments for the four structures considered. Comparing the calculated phonon frequencies for the fully relaxed structure [column (a)] with those measured by Burns *et al.* on ceramic samples,[39] also given in Table IV, we find excellent agreement. The calculations allow us to confirm the mode assignments of the A_{2u}(TO1) and E_u(TO3): Burns' suggestion of assigning the lower mode at 242-cm^{-1} A_{2u} symmetry and the higher mode at 259-cm^{-1} E_u symmetry appears to

TABLE IV. Phonon frequencies (cm^{-1}) and mode assignments for Sr_2TiO_4. Symmetry labels follow the convention of Ref. 53. Experimental values are from Ref. 39.

Mode	Expt.	(a)	(b)	(c)	(d)
Raman					
A_{1g}	205	216	217	214	200
A_{1g}	578	588	594	588	562
E_g	124	121	118	115	106
E_g	286	271	268	266	263
Infrared					
A_{2u} (TO1)	242	231	231	227	206
A_{2u} (TO2)		378	391	389	368
A_{2u} (TO3)	545	499	501	496	478
A_{2u} (LO)		252	253	249	233
A_{2u} (LO)	467	479	482	480	472
A_{2u} (LO)	683	684	692	687	658
E_u (TO1)	151	148	134	129	117
E_u (TO2)	197	218	211	208	198
E_u (TO3)	259	246	247	244	230
E_u (TO4)		611	590	581	554
E_u (LO)	182	184	180	177	168
E_u (LO)	239	227	225	223	216
E_u (LO)	467	451	450	448	443
E_u (LO)	727	789	766	756	727
Silent					
B_{2u}		303	310	310	303

TABLE V. Dynamical matrix eigenvectors ξ_m of Sr_2TiO_4 for the fully relaxed structure with $a = 3.822$ Å and $c = 12.32$ Å. The corresponding eigendisplacement in real space can be obtained by dividing each value by the appropriate mass factor $\sqrt{M_i}$. Modes A_{1g}, A_{2u}, and B_{2u} involve motion along [001], while the twofold degenerate modes E_g and E_u involve motion along [100] and equivalently along [010].

		Eigenmodes						
Mode	Frequency	Ti	O_y	O_x	Sr(1)	Sr(2)	$O_z(1)$	$O_z(2)$
Raman								
A_{1g}	216	0	0	0	−0.71	0.71	0.03	−0.03
A_{1g}	588	0	0	0	−0.03	0.03	−0.71	0.71
E_g	121	0	0	0	−0.70	0.70	−0.06	0.06
E_g	271	0	0	0	0.06	−0.06	−0.70	0.70
Infrared								
A_{2u} (TO1)	231	0.48	0.38	0.38	−0.44	−0.44	0.23	0.23
A_{2u} (TO2)	378	−0.77	0.29	0.29	0.01	0.01	0.34	0.34
A_{2u} (TO3)	499	0.11	−0.46	−0.46	−0.07	−0.07	0.53	0.53
E_u (TO1)	148	0.14	0.11	0.24	−0.37	−0.37	0.56	0.56
E_u (TO2)	218	−0.77	−0.29	−0.14	0.24	0.24	0.31	0.31
E_u (TO3)	246	0.45	−0.86	−0.19	0.02	0.02	0.09	0.09
E_u (TO4)	611	0.16	0.32	−0.91	0.00	0.00	0.14	0.14
Silent								
B_{2u}	303	0	0.71	−0.71	0	0	0	0

be correct. In addition, Burns' assessment that the strong LO feature at ≈ 440 cm^{-1} in the measured reflectivity spectra was ''probably'' due to both a A_{2u}(LO) and a E_u(LO) mode is consistent with our calculations, where we found $A_{2u}(\mathrm{LO}) = 479$ cm^{-1} and $E_u(\mathrm{LO}) = 451$ cm^{-1}.[41] In fact, an average of these two frequencies is within 2 cm^{-1} of the quoted value 467 cm^{-1}. Finally, we obtain the frequencies of four modes that could not be separately identified in the experiment, namely the A_{2u}(TO2) mode at 378 cm^{-1}, the A_{2u}(LO) mode at 252 cm^{-1}, the E_u(TO4) mode at 611 cm^{-1}, and the B_{2u} mode at 303 cm^{-1}.

In Table V we give the normalized dynamical matrix eigenvectors for the fully relaxed structure (a). We see that the lowest frequency A_{2u}(TO1) and E_u(TO1) modes involve Sr atoms moving against a fairly rigid TiO_6 octahedron, with larger deformation of the octahedron for the E_u mode. The highest frequency A_{2u}(TO3) and E_u(TO4) modes each involve large distortions of the oxygen octahedra with the apical oxygens moving against the planar oxygens in the A_{2u} mode and a corresponding distortion for the E_u mode. The calculated A_{2u}(TO2) mode involves Ti atoms moving against a nearly rigid oxygen octahedron, giving rise to a relatively large mode effective charge. Finally, the E_u(TO2) mode, characterized by Burns *et al.* as a weak infrared active mode, has displacements of O_y and O_z very close to those of the triply degenerate silent mode in the cubic perovskite. These patterns are substantially different from those obtained in model calculations of the lattice dynamics of K_2ZnF_4,[42] used by Burns to characterize the eigenvectors of Sr_2TiO_4, especially for the highest frequency A_{2u}(TO3) and E_u(TO4) modes and the A_{2u}(TO2) mode.

The effective plasma frequencies (Sec. II C) are reported in Table VI. There is relatively little variation among the different modes of the same symmetry in the same structure, with $\Omega_{p,m} \approx 400$ and 800 cm^{-1} for the A_{2u} and E_u, respectively, and even less variation with changes in the structure. The largest calculated effective plasma frequency is obtained for the A_{2u}(TO2) mode. While the corresponding oscillator strength, which goes like $\Omega_{p,m}^2$, should make this the most prominent mode in a single-crystal infrared study, it was not

TABLE VI. Effective plasma frequency $\Omega_{p,m}$ (cm^{-1}) and mode contribution to the static dielectric tensor $\Delta\epsilon_m$ in Sr_2TiO_4.

	(a)			(b)			(c)			(d)		
Mode	ω_m	$\Omega_{p,m}$	$\Delta\epsilon_m$	ω_m	$\Omega_{p,m}$	$\Delta\epsilon_m$	ω_m	$\Omega_{p,m}$	$\Delta\epsilon_m$	ω_m	$\Omega_{p,m}$	$\Delta\epsilon_m$
A_{2u}(TO1)	231	457	3.93	231	446	3.71	227	449	3.93	206	474	5.28
A_{2u}(TO2)	378	1061	7.86	391	1066	7.42	389	1073	7.62	368	1083	8.66
A_{2u}(TO3)	499	427	0.73	501	447	0.80	496	409	0.68	478	232	0.24
E_u(TO1)	148	752	25.9	134	809	36.4	129	829	41.0	117	888	57.24
E_u(TO2)	218	473	4.69	211	491	5.41	208	507	5.95	198	586	8.80
E_u(TO3)	246	794	10.4	247	745	9.08	244	723	8.78	230	617	7.21
E_u(TO4)	611	812	1.77	590	759	1.65	581	737	1.61	554	674	1.48

TABLE VII. Nonzero components of the electronic and the ionic dielectric tensors for Sr_2TiO_4 ($\epsilon_{11}, \epsilon_{22}, \epsilon_{33}$). Experimental measurements on thin films (Ref. 8) and on ceramic samples (Refs. 4, 5 and 9) were conducted at room temperature except for † ($T=15$ K).

	Experimental							
	Ref. 8	Ref. 9	Ref. 4	Ref. 5	(a)	(b)	(c)	(d)
ϵ_∞					(5.09,5.09,4.81)	(5.08,5.08,4.82)	(5.07,5.07,4.82)	(5.08,5.08,4.79)
ϵ_{ionic}					(42.8,42.8,12.5)	(52.6,52.6,11.9)	(57.3,57.3,12.2)	(74.7,74.7,14.2)
ϵ_0					(48,48,17)	(58,58,17)	(62,62,17)	(80,80,19)
$\epsilon_{average}$	44±4	38	34, 37†	37	38	44	47	60

separately identified in the ceramic sample of Burns. In ceramics, while the reststrahlen bands do not overlap for modes transforming as the same irreducible representation, the A_{2u} modes can overlap the E_u and vice versa. In fact, we see that not only the A_{2u}(TO2) mode, but also a second high-oscillator strength mode, E_u(TO4), not identified in the measurements of Burns, lie in the middle of a wide reststrahlen band of the other symmetry type. As noted by Burns, this would undoubtedly complicate the interpretation of the reflectivity spectrum and may explain why neither of these modes were identified.

D. Dielectric permittivity tensors

Here we present our calculation of the static dielectric permittivity tensor ϵ_0 for the structures considered in Table II. By the symmetry of the Sr_2TiO_4 structure we see that the tensors are diagonal and have two independent components, along directions parallel to and perpendicular to the TiO_2 layers. In Table VII we display the results of our calculations for these three tensors (ϵ_∞, ϵ_{ionic}, and ϵ_0) for Sr_2TiO_4 under the various structural constraints previously discussed (see the caption of Table II). It can be seen that the static dielectric permittivity tensor is quite anisotropic, with the in-plane components nearly three times as large as the component along [001].

To improve our understanding of this anisotropy we examine the contribution to ϵ_{ionic} from individual phonon modes. In Table VI we show the effective plasma frequency $\Omega_{p,m}$ and the contribution to the static dielectric permittivity for each IR-active phonon mode, equal to $\Omega^2_{p,m}/\omega^2_m$. The A_{2u} and the E_u modes contribute to the components of ϵ_0 along directions perpendicular and parallel to the TiO_2 layers, respectively. We see that the dominant mode contributing to the rather large anisotropy is the E_u(TO1) mode, while the largest $\Omega_{p,m}$ is associated with the A_{2u}(TO2) mode. In fact, the effective plasma frequency of the A_{2u}(TO2) mode is ~40% larger than that of the E_u(TO1) mode. The fact that the frequency of this A_{2u}(TO2) mode is more than twice that of the soft E_u(TO1) mode explains its relatively small contribution to the dielectric permittivity tensor.

Finally, to compare the calculated dielectric permittivity tensors with the measured dielectric constant of the ceramic samples ϵ_r, we compute an orientational average $\epsilon_{average}$ of our calculated results. From Table VII we see that $\epsilon_{average}=38$ for the fully relaxed structure agrees quite well with $\epsilon_r=34$–38 measured by the various groups. The comparison with the thin-film results is more problematic and will be discussed in the next section.

IV. DISCUSSION

In this section, we discuss the main features of the $T=0$ dielectric response of Sr_2TiO_4. We show that the anisotropy and sensitivity to changes in the lattice constants through epitaxial strain and thermal expansion can be understood by relating the dielectric response of Sr_2TiO_4 to that of $SrTiO_3$. Finally, we discuss the comparison of the results of our calculations to available experimental data.

First, we consider the Born effective charges. In $SrTiO_3$, the anomolously large Born effective charges for Ti and O (Table VIII) can be directly linked to the presence of infinite Ti-O chains running in all three Cartesian directions. [43,44] In Sr_2TiO_4 the infinite Ti-O chains lying in the TiO_2 planes are preserved, while the Ti-O chains along [001] are broken into short O-Ti-O segments by the relative shift of the SrO-terminated perovskite slabs [see Fig. 1(c)]. Correspondingly, as can be seen in Table III, the Z^*'s in Sr_2TiO_4 for Ti and O displacing along the infinite chains in the TiO_2 layers, $Z^*_{yy}(\mathrm{Ti})[Z^*_{xx}(\mathrm{Ti})]$ and $Z^*_{yy}(\mathrm{O}_y)[Z^*_{xx}(\mathrm{O}_x)]$, are only slightly smaller than those of $SrTiO_3$.[45] In contrast, the breaking of the Ti-O chains into O-Ti-O segments along [001] has a dramatic effect on the anomalous component of the Ti and O Born effective charges for motion along the segment, $Z^*_{zz}(\mathrm{Ti})$ and $Z^*_{zz}(\mathrm{O}_z)$, reducing them by over a factor of 2. While it is

TABLE VIII. The structural and dielectric properties of $SrTiO_3$ calculated within present theory ($6\times6\times6$ grid, 45 Hartree).

Lattice constant	phonons (cm^{-1})	ω_m	$\Delta\epsilon_m$	$\Omega_{p,m}$
$a=3.846$ Å	T_{1u}(TO1)	103	1275	153
Born effective charge	T_{1u}(TO2)	189	827	19.2
$Z^*(\mathrm{Ti})=7.26$	T_{1u}(TO3)	587	946	2.6
$Z^*(\mathrm{Sr})=2.55$	T_{1u}(LO1)	166		
$Z^*(\mathrm{O}_\perp)=-2.04$	T_{1u}(LO2)	451		
$Z^*(\mathrm{O}_\parallel)=-5.72$	T_{1u}(LO3)	822		
Dielectric constant				
$\epsilon^\infty=6.2$, $\epsilon_0=181$				
Phonon eigenvector	$\{\xi_{Ti}, \xi_{Sr}, \xi_{O\parallel}, \xi_{O\perp}, \xi_{O\perp}\}$			
T_{1u}(TO1)	{−0.14,−0.51, 0.37, 0.54, 0.54}			
T_{1u}(TO2)	{0.84,−0.51,−0.02−0.12,−0.12}			
T_{1u}(TO3)	{0.10, 0.02,−0.88, 0.33. 0.33}			

true that the local anisotropy caused by the somewhat larger Ti-O_z bond length compared with the Ti-O_y bond length will also reduce the corresponding Born effective charges, this is a much weaker effect, as suggested by the following calculation. We fixed the Ti-O_z distance to that of the Ti-O_y bond length of structure (b) (where the in-plane plane lattice parameter was fixed to the lattice constant of $SrTiO_3$), creating a structure whereby the Ti-O distances are equal in all three cartesian directions. The Born effective charges along [001] were found to increase compared with those of Table III(b), but only slightly [$Z^*_{zz}(\mathrm{Ti})=5.29$ and $Z^*_{zz}(\mathrm{O}_z)=-3.80$].

This reduction of the anomalous component of the Born effective charges is quite similar to the reduction of the Z^*'s observed in $BaTiO_3$ due to the ferroelectric transition. Indeed, Ghosez *et al.*[37,46] found that $Z^*(\mathrm{Ti})=7.29$ and $Z^*(\mathrm{O}_\parallel)=-5.75$ in cubic $BaTiO_3$ while in the tetragonal phase they found $Z^*_{yy}(\mathrm{Ti})=6.94$, $Z^*_{yy}(\mathrm{O}_y)=-5.53$, $Z^*_{zz}(\mathrm{Ti})=5.81$, and $Z^*_{zz}(\mathrm{O}_z)=-4.73$. It was explained that this reduction of the Z^*'s going from the cubic to the tetragonal phase resulted from the displacement of the Ti atom along the ferroelectric axis, resulting in a series of long-short Ti-O bonds thereby ''breaking'' the Ti-O chains.[46] In Sr_2TiO_4 this breaking of the Ti-O chains can be thought of as being caused not by alternating Ti-O bond lengths along a given direction, but by the shift of the SrO-terminated $SrTiO_3$ slabs, resulting in a SrO-SrO antiphase boundary perpendicular to [001] as discussed in Sec. III A. Finally, this breaking of the chains in Sr_2TiO_4 is arguably a much ''stronger'' effect than the cubic-to-tetragonal transition in $BaTiO_3$, as evidenced by the greater reduction of the Born effective charges along [001].

We now consider the frequencies and eigenvectors of the infrared active modes of the dynamical matrix. In Table VI, it can be seen that the large in-plane response in Sr_2TiO_4 is dominated by the E_u(TO1) mode. This mode has displacements in the SrO-terminated perovskite slab, so that the longitudinal nearest neighbors of each atom are arranged as in $SrTiO_3$. The primary difference is in the atomic arrangements and transverse force constants between atoms in adjacent slabs. As a result, the frequency is low, though not as low as that of the T_{1u}(TO1) mode in $SrTiO_3$. The relationship of this E_u(TO1) mode in Sr_2TiO_4 to the T_{1u}(TO1) mode in $SrTiO_3$ is further evidenced by its similar high sensitivity to the lattice constant.[47,48] With the change in a from 3.822 Å [case (a)] to 3.88 Å [case (d)], the mode significantly softens, leading to an increase in the in-plane component of the dielectric tensor by over a factor of two.

In contrast, the A_{2u} TO modes involve displacements out of the perovskite slab, so that the longitudinal nearest neighbor arrangements of the Sr and O_z atoms are distinct from those in $SrTiO_3$. As a result, these modes are much more affected than the E_u TO modes by the change in structure relative to $SrTiO_3$. There is no mode with very low frequency, and the mode-by-mode contributions to the dielectric tensor, even that of the A_{2u} (TO2) mode with its large oscillator strength, are modest. As can be seen from Table VI, these modes are rather insensitive to the in-plane lattice constant, with a corresponding constancy in ϵ_{33}.

These observations should generalize, at least semiquantitatively, to higher RP phases (with $n>1$) of Sr-Ti-O. For instance, the anomalous contribution to the Born effective charge tensors of Ti and of O along directions parallel to the O-Ti-O segment should increase with n, but always be lower than those along the infinite chains. As the perovskite slabs get thicker, the ''surface'' effects on the eigenmodes due to the different enviroments of the Sr and O atoms in the outer layer should decrease. The low-frequency in-plane modes should increasingly resemble those of $SrTiO_3$. Most significantly, the frequencies of the lowest A_{2u} modes should decrease, the result being that the overall anisotropy will decrease and reach the isotropic limit as $n\rightarrow\infty$. Because structural modifications to the internal parameters (u', v, and δ_{SrO}), in addition to changes in lattice parameters (a and c), are to be expected with structures of increasing n, the question of how exactly these quantities change with n cannot be answered without full first-principles calculations on higher RP structures.[49] Similar considerations should apply for other titanate perovskite-related materials, and could be used in the theoretical design of new dielectric materials.

Anisotropy of the dielectric tensor has not been previously experimentally determined in Sr_2TiO_4, though measurements have been carried out for single crystals of three isostructural oxides $CaYAlO_4$, $CaNdAlO_4$, and $LaSrAlO_4$.[50] For all three, the anisotropy is very small (for $LaSrAlO_4$, the out-of-plane component of the dielectric tensor, $\epsilon_{33}=20.02$, is in fact slightly greater than the in-plane component $\epsilon_{11}=\epsilon_{22}=16.81$). These values are similar to that of the out-of-plane component of the dielectric tensor of Sr_2TiO_4. The large anisotropy in Sr_2TiO_4 is thus seen to arise from the $SrTiO_3$-related low-frequency in-plane mode, highlighting the unique physics of the mixed covalent-ionic Ti-O bonding in the titanate perovskites.

The anisotropy of the dielectric tensor is an important factor to be taken into consideration when comparing the computed dielectric response with experiment, and, indeed, in correctly interpreting experimental measurements. For ceramics, anisotropy of the single-crystal response can give a range of values for the measured dielectric response, depending on the size, shape, and interaction of the grains. In the single-crystal films, the anisotropy complicates the interpretation of the microwave microscope method of determining the dielectric response. The effective dielectric constant obtained by this technique is in fact an average of the dielectric tensor components determined by the field distribution near the probe, which is itself determined by the anisotropic dielectric response. While an exact value requires detailed modeling of the field configuration, the expectation is that the measured value should be an average weighted in favor of the high dielectric response components. Thus the value $\epsilon_{eff}=44$ obtained by Haeni[8] is not ϵ_{33}, but is a weighted average of the three components, in accordance with our calculations. The agreement of this ϵ_{eff} with the low-frequency electronic measurement is apparently coincidental. The latter measurement determines ϵ_{33}, but at low frequencies it is not unusual for additional extrinsic contributions to raise the value of the dielectric response.

V. SUMMARY

We have investigated the structural and dielectric properties of Sr_2TiO_4, the first member of the $Sr_{n+1}Ti_nO_{3n+1}$ Ruddlesden-Popper series, within density-functional theory. Density-functional perturbation theory was used to compute the zone-center phonon frequencies, Born effective charges, and the electronic dielectric permittivity tensor. The structural parameters and computed properties generally compare favorably with available experimental and previous theoretical results.

Our calculation of the static dielectric tensor of Sr_2TiO_4 from the above data provides valuable information about the anisotropy of the response. This anisotropy is key to interpreting the available experimental data on the dielectric response of ceramic and thin-film samples. The anisotropy in this system is seen to arise from a low-frequency in-plane mode closely related to that in $SrTiO_3$. This picture should generalize to the higher RP phases of Sr-Ti-O as well as other titanate perovskite-related materials, and could be useful in tailoring the dielectric response of this class of materials.

ACKNOWLEDGMENTS

The authors would like to acknowledge valuable discussions with Darrell Schlom, David Vanderbilt, and Morrel Cohen. This work was supported by NSF-NIRT Grant No. DMR-0103354.

[1] R.J.D. Tilley, J. Solid State Chem. **21**, 293 (1977).
[2] S.N. Ruddlesden and P. Popper, Acta Crystallogr. **10**, 538 (1957).
[3] G. McCarthy, W.R. White, and R. Roy, J. Am. Ceram. Soc. **52**, 463 (1969).
[4] J.H. Sohn, Y. Inaguma, M. Itoh, and T. Nakamura, Ferroelectrics **166**, 149 (1995); Mater. Sci. Eng., B **41**, 50 (1996).
[5] P.L. Wise, I.M. Reaney, W.E. Lee, T.J. Price, D.M. Iddles, and D.S. Cannell, J. Eur. Ceram. Soc. **21**, 2629 (2001); **21**, 1723 (2001); J. Mater. Res. **17**, 2033 (2002).
[6] S.N. Ruddlesden and P. Popper, Acta Crystallogr. **11**, 54 (1958).
[7] W. Tian, X.Q. Pan, J.H. Haeni, and D.G. Schlom, J. Mater. Res. **16**, 2013 (2001).
[8] J.H. Haeni, C.D. Theis, D.G. Schlom, W. Tian, X.Q. Pan, H. Chang, I. Takeuchi, and X.D. Xiang, Appl. Phys. Lett. **78**, 3292 (2001).
[9] W. Kwestroo and H.A.M. Paping, J. Am. Ceram. Soc. **42**, 292 (1959).
[10] T. Nakamura, P.-H. Sun, Y.J. Shan, Y. Inaguma, M. Itoh, I.-S. Kim, J.-H. Sohn, M. Ikeda, T. Kitamura, and H. Konagaya, Ferroelectrics **196**, 205 (1997).
[11] S. Baroni, S. de Gironcoli, A. Dal Corso, and P. Giannozzi, Rev. Mod. Phys. **73**, 515 (2001).
[12] X. Gonze, J.-M. Beuken, R. Caracas, F. Detraux, M. Fuchs, G.-M. Rignanese, L. Sindic, M. Verstraete, G. Zerah, F. Jollet, M. Torrent, A. Roy, M. Mikami, Ph. Ghosez, J.-Y. Raty, and D.C. Allan, Comput. Mater. Sci. **25**, 478 (2002).
[13] ABINIT is a common project of the Université Catholique de Louvain, Corning Incorporated and other contributors (URL http://www.abinit.org). It relies on an efficient fast Fourier transform algorithm (Ref. 54) for the conversion of wave functions between real and reciprocal space, on the adaptation to a fixed potential of the band-by-band conjugate gradient method (Ref. 55), and on a potential-based conjugate-gradient algorithm for the determination of the self-consistent potential (Ref. 56). Technical details of the computation of responses to atomic displacements and homogeneous electric fields can be found in Ref. 21, while Ref. 22 presents the subsequent computation of dynamical matrices, Born effective charges, dielectric permittivity tensors, and interatomic force constants.
[14] D.M. Ceperley and B.J. Alder, Phys. Rev. Lett. **45**, 566 (1980).
[15] H.J. Monkhorst and J.D. Pack, Phys. Rev. B **13**, 5188 (1976); **16**, 1748 (1977).
[16] H.B. Schlegel, J. Comput. Chem. **3**, 214 (1982).
[17] Calculations were performed on a $6\times6\times6$ grid at an energy cutoff of 45 Hartree (Ha), following the approach described in Sec. II A.
[18] D. Vanderbilt, Curr. Opin. Solid State Mater. Sci. **2**, 701 (1997).
[19] Na Sai and David Vanderbilt, Phys. Rev. B **62**, 13 942 (2000).
[20] F.W. Lytle, J. Appl. Phys. **35**, 2212 (1964).
[21] X. Gonze, Phys. Rev. B **55**, 10 337 (1997).
[22] X. Gonze and Ch. Lee, Phys. Rev. B **55**, 10 355 (1997).
[23] G.-M. Rignanese, X. Gonze, and A. Pasquarello, Phys. Rev. B **63**, 104305 (2001).
[24] G.-M. Rignanese, F. Detraux, X. Gonze, and A. Pasquarello, Phys. Rev. B **64**, 134301 (2001).
[25] M. Born and K. Huang, *Dynamical Theory of Crystal Lattices* (Oxford University Press, Oxford, 1954).
[26] A.A. Maradudin, E.W. Montroll, G.H. Weiss, and I.P. Ipatova, in *Solid State Physics: Advances in Research and Applications*, edited by H.E. Ehrenreich, F. Seitz, and D. Turnbull (Academic, New York, 1971), Suppl. 3, Chap. 4.
[27] J.M. Ziman, *Principles of the Theory of Solids*, 2nd ed. (Cambridge University Press, Cambridge, England, 1972).
[28] D.Y. Smith, in *Handbook of Optical Constants of Solids*, edited by E.D. Palik (Academic Press, New York, 1985), pp. 35–68.
[29] X. Zhao and D. Vanderbilt, Phys. Rev. B **65**, 075105 (2002).
[30] X. Zhao and D. Vanderbilt, Phys. Rev. B **65**, 233106 (2002).
[31] E. Cockayne and B.P. Burton, Phys. Rev. B **62**, 3735 (2000).
[32] The mode effective charge, if defined as the constant of proportionality between the induced polarization and a real-space eigendisplacement, is given by $\Sigma_{i\gamma}\ Z^*_{\alpha\gamma}(i)U_m(i\gamma)/[\Sigma_{i\gamma}U^*_m(i\gamma)U_m(i\gamma)]^{1/2}$.
[33] U.V. Waghmare and K.M. Rabe (unpublished).
[34] C. Noguera, Philos. Mag. Lett. **80**, 173 (2000).
[35] U. Venkateswaran, K. Strossner, K. Syassen, G. Burns, and M.W. Shafer, Solid State Commun. **64**, 1273 (1987).
[36] This assumes a *c*-axis lattice parameter ($c=12.60$ Å) equal to that previously reported in the literature for ceramic samples. Note that the *c*-axis lattice parameter is missing from their paper.

[37] Ph. Ghosez, X. Gonze, Ph. Lambin, and J.-P. Michenaud, Phys. Rev. B **51**, 6765 (1995).
[38] C.-Z. Wang, R. Yu, and H. Krakauer, Phys. Rev. B **54**, 11 161 (1996).
[39] G. Burns, F.H. Dacol, G. Kliche, W. Konig, and M.W. Shafer, Phys. Rev. B **37**, 3381 (1988).
[40] G. Burns, F.H. Dacol, and M.W. Shafer, Solid State Commun. **62**, 687 (1987).
[41] In Table II of Ref. 39, the A_{2u} mode and the E_u mode giving rise to the strong LO feature at $\approx$440 cm^{-1} were each assigned a value of 467 cm^{-1}.
[42] H. Rauh and R. Geick, Phys. Status Solidi B **127**, 55 (1985).
[43] W. Zhong, R.D. King-Smith, and D. Vanderbilt, Phys. Rev. Lett. **72**, 3618 (1994).
[44] C. LaSota, C-Z. Wang, R. Yu, and H. Krakauer, Ferroelectrics **194**, 109 (1997).
[45] The hybridization of the Ti $3d$ and O $2p$ states has been shown to be the origin of the anomalous Born effective charges (BEC's) in the perovskites.[57] Because one expects this hybridization, or the rate of change of this hybridization,[37] to depend on the length of the Ti-O bond we should compare BEC's in $SrTiO_3$ and Sr_2TiO_4 at the same bond length.
[46] Ph. Ghosez, J.-P. Michenaud, and X. Gonze, Phys. Rev. B **58**, 6224 (1998).
[47] S. Hyun and K. Char, Appl. Phys. Lett. **79**, 254 (2001).
[48] A.R. James and X.X. Xi, J. Appl. Phys. **92**, 6149 (2002).
[49] C.J. Fennie and K.M. Rabe (unpublished).
[50] R.D. Shannon, R.A. Oswald, J.B. Parise, B.H.T. Chai, P. Byszewski, A. Pajaczkowska, and R. Sobolewski, J. Solid State Chem. **98**, 90 (1992).
[51] T. Suzuki and M. Fujimoto, J. Appl. Phys. **89**, 5622 (2001).
[52] M.A. McCoy, R.W. Grimes, and W.E. Lee, Philos. Mag. A **75**, 833 (1997).
[53] G. Burns and A.M. Glazer, *Space Groups for Solid State Scientists* (Academic Press, New York, 1978).
[54] S. Goedecker, SIAM J. Sci. Comput. (USA) **18**, 1605 (1997).
[55] M.C. Payne, M.P. Teter, D.C. Allan, T.A. Arias, and J.D. Joannopoulos, Rev. Mod. Phys. **64**, 1045 (1992).
[56] X. Gonze, Phys. Rev. B **54**, 4383 (1996).
[57] M. Posternak, R. Resta, and A. Baldereschi, Phys. Rev. B **50**, 8911 (1994).